Engineering Notes

ENGINEERING NOTES are short manuscripts describing new developments or important results of a preliminary nature. These Notes cannot exceed 6 manuscript pages and 3 figures; a page of text may be substituted for a figure or vice versa. After informal review by the editors, they may be published within a few months of the date of receipt. Style requirements are the same as for regular contributions (see inside back cover).

Ablation of Graphite in High-Speed Air Streams

John A. Segletes*
Teledyne Isotopes, Timonium, Md.

Nomenclature

B' = mass addition parameter [see Eq. (2)]
C_H = Stanton number
K = mass fraction
K_p = equilibrium constant
$\tilde{K}_C$ = mass fraction of chemical element carbon
$\tilde{K}_O$ = mass fraction of chemical element oxygen
K'_C = mass fraction of chemical element carbon exclusive of K_{CO}
L_e = Lewis-Semenov number
$\dot{m}$ = mass flux rate
$\bar{M}$ = effective molecular weight
P = pressure
Pr = Prandtl number
R = gas constant
R_n = nose radius
Sc = Schmidt number
T = temperature
u = component of velocity parallel to wall
v = component of velocity perpendicular to wall
α = accommodation coefficient
ρ = density

Subscripts

DL = diffusion limited
e = edge
w = wall

Introduction

THE ablation of graphite in high-speed air streams is a complex phenomenon that has been studied extensively in recent years. If the wall temperature is below 5000°R and the pressure is moderate (0.1 to 10 atm), graphite ablation will be primarily the result of oxidation. Above this threshold temperature sublimation begins to become significant. Sublimation increases rapidly with increases in wall temperature and soon becomes the predominant source of ablation. As the wall temperature rises, so does the vapor pressure. It is therefore possible to achieve a quasi-boiling state if the wall temperature is raised high enough. While boiling, the wall temperature will be a function of vapor pressure only. Because of the very high wall temperature required to achieve graphite boiling, this state is seldom realized in practical applications.

The subject of this paper is the ablation of graphite due to convective heat transfer in the high-wall temperature-moderate pressure region where sublimation represents a significant portion of total ablation. This region, frequently referred to as the sublimation regime, ranges in wall temperature from approximately 5000°R to levels that cause graphite to boil.

The analytical methods used in this study are not new. However, when these results are applied to the graphite sublimation problem, a much better correlation is obtained with experimental data than can be obtained with either one of several published studies on the subject.[1-3] The results of this study suggest that graphite ablation can usually be explained solely on the basis of thermochemical processes.

Models

Two ablation models are used in this study. The primary model explicitly accounts for sublimation whereas the secondary model implies that sublimation has occurred.

In the primary model C_3 is formed in accordance with Eq. 1, a modified version of the Langmuir evaporation relation which accounts for a linear variation of sublimation rate with pressure potential. After subliming, the C_3 remains inert and diffuses from the wall. All other species are in chemical equilibrium at the wall.

$$\dot{m}_{C_3} = \frac{\alpha_{C_3}}{(2\pi R_{C_3} T_w)^{1/2}} (K_p - P)_{C_{3_w}} \tag{1}$$

where $\alpha_{C_3} = 1.0$ (assumed).

The secondary model implies that sublimation has occurred by considering all species to be in chemical equilibrium at the wall. In this model C_3 is also the only carbon species at the wall.

Both models account for oxidation. It is assumed from previous studies[4,5] that oxidation is diffusion limited for wall temperatures above 5000°R. Hence the mass fraction of oxygen at the wall is zero and the only oxidation product is CO. The dissociation of molecular nitrogen is also accounted for in both models.

The assumption of C_3 as being the only sublimation product is made on the basis of data in Ref. 6. This reference shows C_3 to be the predominant carbon species in massively ablating graphite specimens, suggesting that C_3 is formed in the sublimation process and then remains substantially frozen.

As a matter of interest, one set of computations was also made with the secondary model in which carbon species C-C_5 were assumed to be in chemical equilibrium at the wall. These computations also assumed a CN producing reaction at the wall. The true composition of carbon species is expected to be somewhere between the frozen C_3 and the equilibrium C-C_5 compositions considered here.

Mass Transfer

Mass transfer rates are computed by a method developed for a laminar boundary layer when $Le = Pr = Sc = 1.0$.[7] To determine diffusion rates, this method uses the similarity between mass fractions of individual chemical elements and the total enthalpy.

For those species containing oxygen, the following applies:

$$\tilde{K}_{O_e}/\tilde{K}_{O_w} + B' + 1 \tag{2}$$

Received February 21, 1974; revision received December 17, 1974. The work reported here was supported under AEC Contract AT (49-15)-3069.

Index categories: Material Ablation; Thermochemistry and Chemical Kinetics.

*Aerothermal Engineer, Safety and Reliability. Member AIAA.

where $\tilde{K}_{O_e}=0.2314$, $\tilde{K}_{O_w}=0.571\,K_{CO_w}$, and

$$B'=\frac{(\rho v)_w}{\rho_e u_e C_H}=\frac{\dot{m}}{\rho_e u_e C_H}$$

The corresponding equation for those species containing carbon is the following:

$$\tilde{K}_{C_w}=B'/(B'+1) \tag{3}$$

By combining Eqs. (2) and (3) the following is obtained:

$$\dot{m}=\frac{12}{16}\,\frac{\rho_e u_e C_H}{(1-K'_{C_w})}\,(\tilde{K}_{O_e}+\frac{16}{12}K'_{C_w}) \tag{4}$$

The mass flux rate is normalized by dividing Eq. (4) by its diffusion limited value.

$$\frac{\dot{m}}{\dot{m}_{DL}}=\left(\frac{C_H}{C_{H_{DL}}}\right)\left[\frac{1}{(1-K'_C)}\quad\left(\frac{0.1725+K'_C}{0.1725}\right)\right]_w \tag{5}$$

The ratio of Stanton numbers in Eq. (5) is evaluated by Eq. (6) which was derived from Eq. 5a of Ref. 5 and a relationship which approximates the laminar stagnation point curve of Fig. 1 in Ref. 7. The injection of species other than air into the boundary layer is accounted for by a molecular weight ratio correlation used previously.[8]

$$\frac{C_H}{C_{H_{DL}}}=\frac{1}{0.889[1+0.1231(\dot{m}/\dot{m}_{DL})(29/\bar{M})^{0.4}]} \tag{6}$$

Continuity of the sublimation product in the primary model requires that the following be satisfied.

$$(\dot{m}_{C_3})_{\text{sublimation}}=(\dot{m}_{C_3})_{\text{diffusion}} \tag{7}$$

Another requirement is the following:

$$K_{pC_{3_w}}=(\Delta P_{C_3})_{\text{sublimation}}+P_{C_{3_w}} \tag{8}$$

Computational Method

Numerical results for the primary model are obtained by satisfying Eqs. (1, 4, 7, and 8). This is accomplished by first computing a family of solutions of Eqs. (1) and (4) in which $P_{C_{3_w}}$ is varied parametrically between zero and $K_{pC_{3_w}}$. The correct value of $\dot{m}$ is determined graphically by plotting $\dot{m}$ and $\dot{m}_{C_3}$ as a function of P_{C_3} and selecting the value of $\dot{m}$ for which $\dot{m}_{C_3}$ satisfies Eq. (7). Secondary model solutions are obtained by solving Eqs. (5) and (6) simultaneously.

Equilibrium constants are taken from Ref. 9. These are required to evaluate the element mass fractions appearing in Eqs. (4) and (5) and the effective molecular weight appearing in Eq. (6). All numerical computations are made on the IBM 360-91 computer in conjunction with the Thermal Analyzer Program (TAP-3).

Results and Discussion

Normalized ablation rates computed for the primary and secondary C_3 models are compared in Fig. 1. The two solutions are almost identical except for combinations of low pressure ($P\sim 0.1$ atm) and high film coefficient ($\rho_e u_e C_H\sim$ 1.0 lb/ft^2-sec). Only bodies having very small nose radii ($\sim$ 0.001 in.) can achieve this combination of pressure and film coefficient. Since most practical problems deal with nose radii much larger than this, an equilibrium model which does not explicitly account for sublimation should yield accurate results for the entire pressure-wall temperature range considered here. This statement must be tempered, however, in

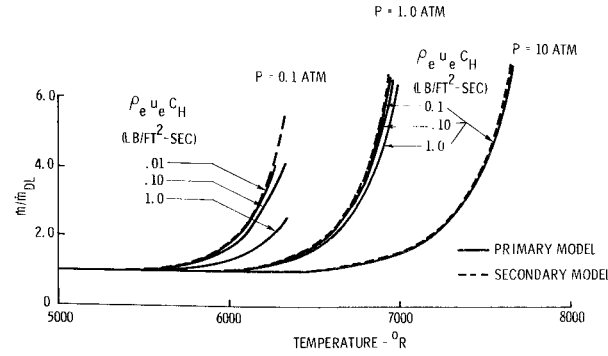

Fig. 1 Normalized graphite ablation; species vaportized; C_3; ablation products: CO; C_3; $Le=Pr=Sc=1.0$.

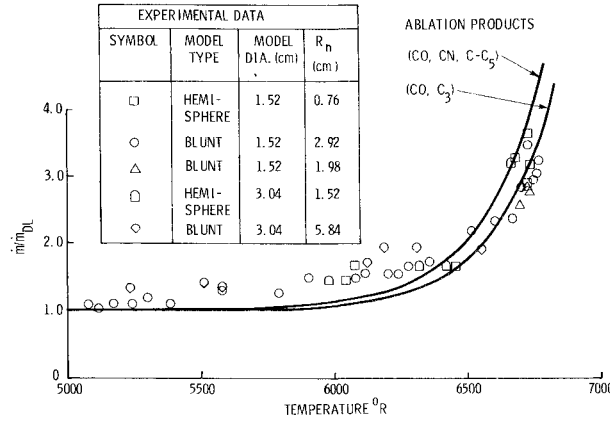

Fig. 2 Correlation with experimental data, $P=1.0$ atm.

view of the $\alpha_{C_3}=1.0$ assumption. Reference 1, for example, shows the α_{C_3} range to be from 0.023 to 0.08. If α_{C_3} is indeed this low, an explicit accounting of sublimation may be required for the analysis of small nosed bodies ($R_n<0.1$ in.) in low pressure ($P<0.1$ atm) regions.

Experimental data reported in Ref. 10 are compared with corresponding analytical results in Fig. 2. The data points shown in Fig. 2 include modifications made to the Ref. 10 data to account for differences between actual test pressures (0.9-1.1 atm) and the one atm pressure level represented in Fig. 2. The correlation suggests that graphite ablation in the sublimation regime can, under normal circumstances, be explained solely on the basis of thermochemical processes. The greatest disparity between the test data and analytical results is in the temperature range where the carbon-nitrogen reaction is most significant, hence suggesting the Ref. 9 equilibrium constants for this reaction may be too low.

A comparison is also made in Fig. 2 between the ablation responses for frozen and equilibrium carbon compositions at the wall. The latter curve also includes the influence of the CN reaction. Relatively little difference exists between the two solutions. This is attributed to the relative insignificance of the CN reaction and the predominance of C_3 over all other carbon species it is in equilibrium with. This comparison suggests carbon species other than C_3 do not influence ablation results to any large degree.

References

[1] Dolton, T. A., Goldstein, H. E., and Maurer, R. E., "Thermodynamic Performance of Carbon in Hyperthermal Environments," *AIAA Progress in Astronautics and Aeronautics: Thermal Design Principles of Spacecraft and Entry Bodies*, Vol. 21, edited by J. Bevans, Academic Press, New York, 1969, pp. 169-201.

[2] Scala, S., and Gilbert, L.M., "Sublimation of Graphite in Air," *AIAA Journal*, Vol. 3, Sept. 1965, pp. 1635-1644.

[3] Kratsch, K. M., Clayton, F. I., Greene, R. B., Martinez, M., and Wuerer, J. E., "Graphite Ablation in High-Pressure Environments," AIAA Paper 68-1153, Williamsburg, Virginia, Dec., 1968.

[4] Welsh, W. E. and Chung, P. M., "A Modified Theory for the Effect of Surface Temperature on the Combustion Rate of Carbon Surfaces in Air," *Proceedings of the Heat Transfer and Fluid Mechanics Institute,* Stanford University Press, 1963, pp. 146-159.

[5] Segletes, J. A., "Oxidation of POCO AXF-Q1 Graphite in Air," *Journal of Spacecraft and Rockets,* Vol. 10, Dec. 1973, pp. 803-806.

[6] Lincoln, K. A., Howe, J. T. and Liu, T., "Assessment of Chemical Nonequilibrium for Massively Ablating Graphite," *AIAA Journal,* Vol. 11, Aug. 1973, pp. 1198-1200.

[7] Lees, L., "Convective Heat Transfer with Mass Addition and Chemical Reactions," *Third AGARD Colloquium,* March 1958.

[8] Adams, M.C., "Recent Advances in Ablation," *ARS Journal,* Vol. 29, Sept. 1959, pp. 625-632.

[9] *JANNAF Thermochemical Tables,* 2nd edi., U.S. Department of Commerce, National Bureau of Standards, NSRDS-NBS 37, June 1971.

[10] Lundell, J. H. and Dickey, R. R., "Graphite Ablation at High Temperatures," *AIAA Journal,* Vol. 11, Feb. 1973, pp. 216-222.

Scheme to Improve Limit Cycle Performance of an Attitude Control System

R. N. Clark* and P. Dumas†
University of Washington, Seattle, Wash.

and

D. C. Fosth‡
Boeing Aerospace Company, Seattle, Wash.

FIGURE 1 is a block diagram of a single axis attitude control system in which an attitude signal, θ^*, is derived by integrating the signal from a precision rate gyro. A stabilizing signal ϵ^* is also derived in the computer

$$\epsilon^* = K_R\omega^* + K_P\theta^*$$

where

$$\theta^* = \int \omega^* dt$$

ϵ^* is used to determine the times at which the thruster is fired, the direction of the thrust, and the duration of the thrust pulse. These three items of intelligence are represented as the valve command, τ_c, in the diagram. The thruster is characterized by the strength of the thrust, A (assumed constant during the pulse), a time delay τ_D between the instant a turn-on command is received and the instant thrust actually occurs, and a minimum time, τ_o, which the pulse width modulator may command as thruster on-time. ω is the angular rate of the vehicle about its controlled axis and is related to the thrust M in the usual way: $M = J\dot{\omega}$. The gyro output signal m_g is dynamically related to the vehicle rate by

$$\ddot{\omega}_g + (2\zeta\omega_n)\dot{\omega}_g + (\omega_n^2)\omega_g = (\omega_n^2)\omega$$

where ζ is the damping ratio and ω_n the undamped natural frequency of the output axis of the gyro. T is the cycle time of the computer, and the analog to digital conversion is represented by a zero order hold, the output of which is ω^*_g, a piecewise constant representation of ω_g.

A conventional method of control for this system is to program the computer to issue a thruster command at each sample instant. The pulse width command at instant t_k is determined from $\epsilon^*(t_k)$ according to the curve in Fig. 2. A dead zone of total width $2W$ is employed to prevent the valve from responding to noise which might exist on the ϵ^* signal. The parameters W, S, K_R, K_P, T, ζ, and ω_n may then all be adjusted to provide acceptable performance of the system where τ_D, τ_o, A, and J are considered fixed.

Insofar as limit cycle performance is concerned these seven parameters are adjusted to minimize control fuel expenditure (total valve on-time) while maintaining acceptable limits on the excursions of ω and θ during the limit cycle oscillation. The conventional control scheme described above leads to a certain optimum limit cycle performance represented qualitatively by the $\epsilon^*(t)$ signal in Fig. 3. Here that portion of the limit cycle during which $\epsilon^*(t)$ reaches its peak is shown. Prior to t_o the vehicle is drifting at a constant rate. t_o is the sample instant at which $\epsilon^*(t)$ first exceeds the dead-zone value W. A pulse width is calculated from Fig. 2 and a thruster command is issued as soon as this calculation is completed. There is a delay, τ_D, between the initiation of the thruster command and the actual occurance of thrust. Also, the gyro does not

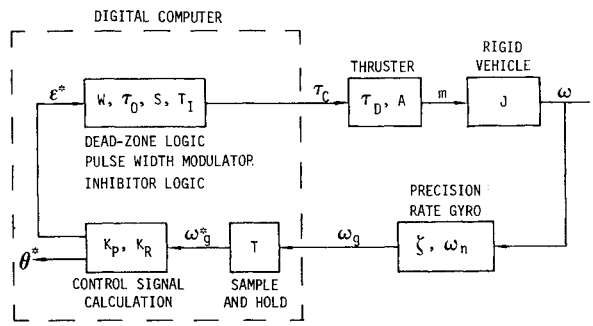

Fig. 1 Single axis attitude control system.

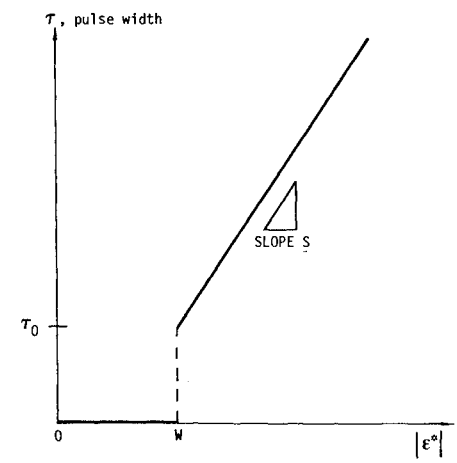

Fig. 2 Pulse-width modulation.

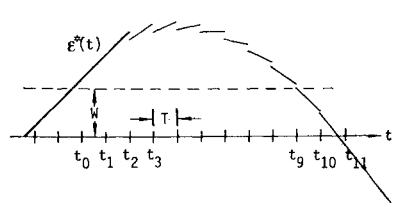

Fig. 3 $\epsilon^*(t)$ vs t during its reversal.

Received October 21, 1974; revision received January 14, 1975.
Index category: Spacecraft Attitude Dynamics and Control.

*Professor of Electrical Engineering. Also Consultant, Boeing Aerospace Co., Sensors, Guidance, and Control Dept.
†Graduate Student of Electrical Engineering.
‡Engineering Manager, Sensors, Guidance, and Control Dept.